MOLECULAR AND CELLULAR BIOLOGY, Jan. 2007, p. 244–252 Vol. 27, No. 1
0270-7306/07/$08.00+0 doi:10.1128/MCB.00561-06

Targeted Deletion of the Muscular Dystrophy Gene *myotilin* Does Not Perturb Muscle Structure or Function in Mice▽

Monica Moza,[1]* Luca Mologni,[1]† Ras Trokovic,[2]‡ Georgine Faulkner,[3] Juha Partanen,[2] and Olli Carpén[1,4]

Department of Pathology and Neuroscience Program, Biomedicum Helsinki, P.O. Box 63, Haartmaninkatu 8, 00014 University of Helsinki, Helsinki, Finland[1]; Institute of Biotechnology, Viikki Biocenter, Developmental Biology Program, P.O. Box 56, Viikinkaari 9, 00014 University of Helsinki, Helsinki, Finland[2]; International Center for Genetic Engineering and Biotechnology, Padriciano 99, Trieste, Italy[3]; and Department of Pathology, University of Turku, and Turku University Central Hospital, Kiinamyllynkatu 10, 20520 Turku, Finland[4]

Received 30 March 2006/Returned for modification 27 May 2006/Accepted 17 October 2006

Myotilin, palladin, and myopalladin form a novel small subfamily of cytoskeletal proteins that contain immunoglobulin-like domains. Myotilin is a thin filament-associated protein localized at the Z-disk of skeletal and cardiac muscle cells. The direct binding to F-actin, efficient cross-linking of actin filaments, and prevention of induced disassembly of filaments are key roles of myotilin that are thought to be involved in structural maintenance and function of the sarcomere. Missense mutations in the myotilin-encoding gene cause dominant limb girdle muscular dystrophy type 1A and spheroid body myopathy and are the molecular defect that can cause myofibrillar myopathy. Here we describe the generation and analysis of mice that lack myotilin, *myo*$^{-/-}$ mice. Surprisingly, *myo*$^{-/-}$ mice maintain normal muscle sarcomeric and sarcolemmal integrity. Also, loss of myotilin does not cause alterations in the heart or other organs of newborn or adult *myo*$^{-/-}$ mice. The mice develop normally and have a normal life span, and their muscle capacity does not significantly differ from wild-type mice even after prolonged physical stress. The results suggest that either myotilin does not participate in muscle development and basal function maintenance or other proteins serve as structural and functional compensatory molecules when myotilin is absent.

The muscle sarcomere is a strictly organized cytoskeletal structure responsible for force generation and transmission. The sarcomeric actin-containing thin filaments are aligned and anchored by the Z-disks, specialized three-dimensional structures composed of multiprotein complexes. In addition to thin filaments, Z-disks anchor laterally the sarcomere to the sarcolemma. Recently, several novel disease entities caused by inherited mutations in Z-disk proteins have been identified. Among these are myotilinopathies, muscular disorders caused by missense mutations in the Z-disk protein myotilin (7, 12, 13, 28, 36). Myotilinopathies are characterized by proximal and/or distal muscle weakness, occasionally cardiomyopathy, elevated serum creatine kinase levels, and reduced tendon reflexes. Typical morphological features include extensive disruption of the myofibrillar architecture, Z-disk streaming, and accumulation of apparently Z-disk-associated filamentous material. All known myotilinopathies are caused by missense mutations in the amino terminus of myotilin, and they are dominantly inherited and fully penetrant.

Myotilin, together with palladin and myopalladin, forms a small subfamily of immunoglobulin (Ig)-like domain-containing cytoskeletal proteins (25). While the carboxy terminus of myotilin is highly conserved within the subfamily, its amino terminus is unique and rich in serine residues. Myotilin is mainly expressed in the skeletal and cardiac muscle (21, 33), and it interacts with several structural Z-disk proteins, including α-actinin (33), actin (34, 41), filamin C (40), and FATZ-1 (calsarcin-2/myozenin-1) and FATZ-2 (calsarcin-1/myozenin-2) (10). The association with FATZ links myotilin to the calcineurin signaling pathway, while an interaction with MURF-1 and MURF-2 could involve myotilin in the titin-based signaling events (42). Although myotilin does not contain a conventional actin-binding domain, it is an efficient F-actin cross-linker in vitro and in vivo (34, 41) and, thereby, it may control sarcomere integrity. Indeed, expression of myotilin fragments in muscle cells leads to defective sarcomere maturation, as typical periodical alignment of the contractile proteins is not observed upon differentiation (34, 40).

Murine and human myotilin are highly homologous and share an expression pattern (21), suggesting a conserved evolutionary function. Abundant transcription of the *myotilin* gene in the early embryonic stages of mouse development (21, 22) suggests that it may have an involvement in early stages of skeletal and cardiac muscle formation and function. To investigate the consequences of myotilin deficiency, we generated a myotilin knockout mouse (*myo*$^{-/-}$) by standard techniques of homologous recombination in embryonic stem (ES) cells and a Cre-*loxP*-mediated conditional gene targeting approach. We report here that, surprisingly, loss of myotilin does not lead to

* Corresponding author. Mailing address: Neuroscience Program and Department of Pathology, Biomedicum Helsinki, Haartmaninkatu 8, P.O. Box 63, 00014 University of Helsinki, Helsinki, Finland. Phone: 358-9-19125652. Fax: 358-9-47171964. E-mail: monica.moza@helsinki.fi.
† Present address: University of Milan-Bicocca, Milan, Italy.
‡ Present address: Program of Developmental and Reproductive Biology, Biomedicum Helsinki, University of Helsinki, Helsinki, Finland.
▽ Published ahead of print on 30 October 2006.

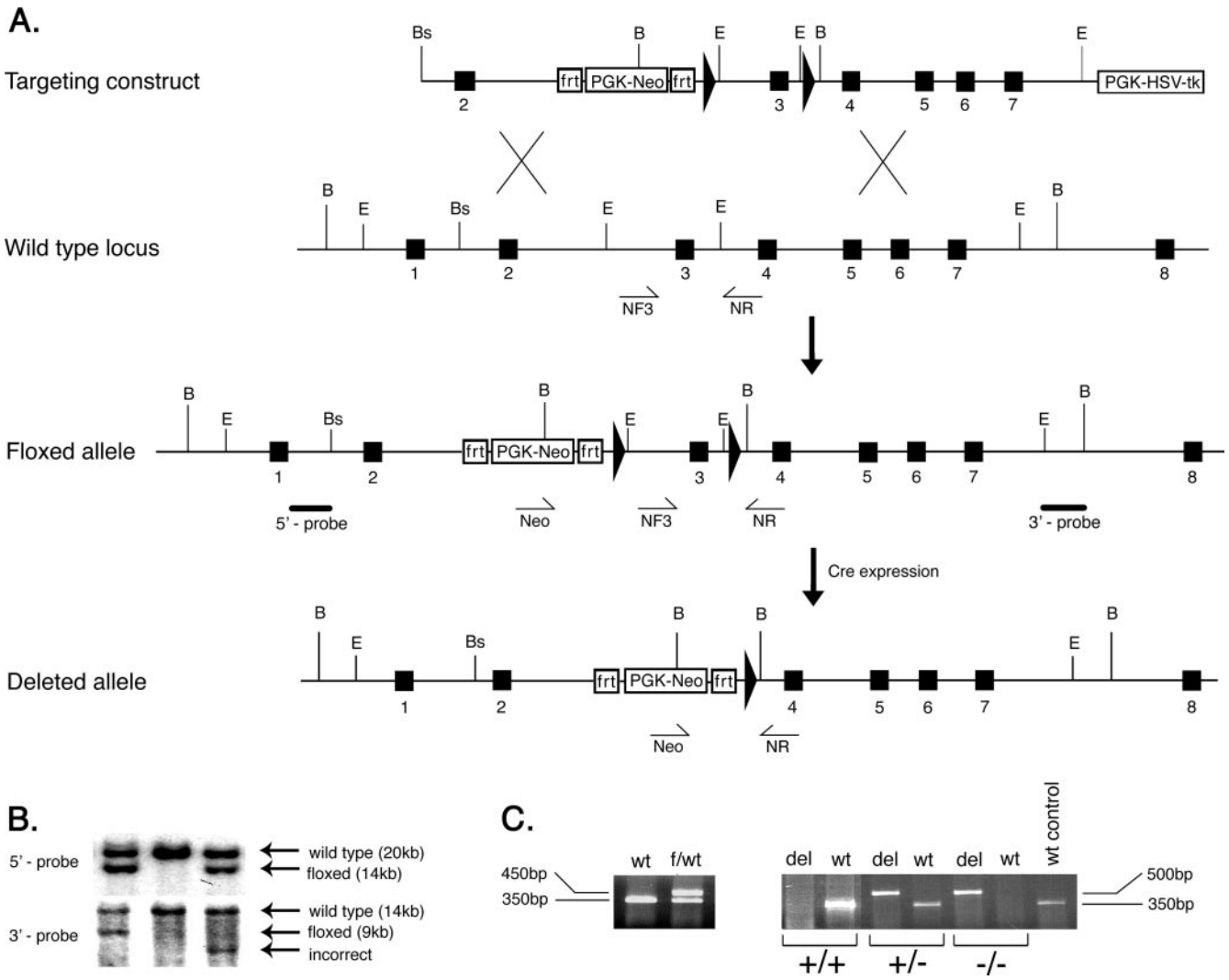

FIG. 1. Generation of the myotilin-deleted allele (*myo*$^{-/-}$). A. The top diagram shows the targeting vector constructed by subcloning genomic myotilin fragments into the pDELBOY-3X vector. The exons are depicted by filled boxes, and the *loxP* sites are shown as filled arrows. Relevant restriction site positions are marked by letters as follows: B, BamHI; E, EcoRI; Bs, BssI. The second diagram shows partial genomic organization of the wild-type murine *myotilin* gene. NF3 and NR represents the relative positions of the genotyping primers used to detect the wild-type allele. The third diagram shows the organization of the conditional (floxed) allele after homologous recombination in ES cells. The solid bars below the intronic regions represent the 5′ and 3′ probes used for detection of correct recombination. The bottom diagram shows the final organization of conditionally deleted *myotilin* gene, missing exon 3. The deletion was obtained in vivo by crossing the mouse bearing the *flox* allele with a Cre-expressing mouse. The Neo and NR primers used for genotyping and detection of the deleted allele are shown schematically as arrows under the genomic locus. PGK-HSV-tk, herpes simplex virus type I thymidine kinase under the phosphoglycerine kinase promoter cassette; PGK-Neo, neomycin gene under the phosphoglycerine kinase promoter. The PKG-Neo cassette is flanked by two frt sites. B. Southern blot of BamHI-digested genomic DNA from three ES clones. The upper panel represents the autoradiography after hybridization with the 5′ probe, shown in panel A. The expected recombination events are observed in the left and right lane, where the wild-type allele of 20 kb and the floxed allele of 14 kb are indicated by arrows. The middle lane shows the control wild-type alleles. In the lower panel, detection of the recombination was done using the 3′ probe. The left lane shows correct recombination events by detection of the wild-type allele of 14 kb and the floxed allele of 9 kb. The middle lane shows only the wild-type allele, and the right lane depicts incorrect recombination events. C. The left panel shows a 350-bp fragment from the wild type (wt) and 450 bp from the floxed allele (f) generated in one PCR with primers NF3 and NR. The right panel shows the genotype of the mice after in vivo Cre-mediated recombination. Wild-type (+) and deleted (−) alleles were detected using two PCRs for each sample. Primers Neo and NR generate a 350-bp fragment from the wild type and 500 bp from the deleted allele (del). The right lane shows a wild-type (+) control reaction.

morphological or physiological abnormalities of striated muscle, heart, or other tissues during the entire life span of *myo*$^{-/-}$ mice. However, we observed in striated muscle the upregulation of telethonin, a small Z-disk protein mutated in an autosomal recessive form of limb girdle muscular dystrophy (LGMD), LGMD2G (23).

MATERIALS AND METHODS

Generation of myotilin null (*myo*$^{-/-}$) mice. The mouse *myotilin* gene-targeting strategy is shown in Fig. 1A. The gene was isolated from a mouse genomic library prepared from 129/SvJ mouse DNA (Research Genetics) using a full-length mouse cDNA as probe. Three genomic fragments encompassing myotilin exons 2 through 7 were subcloned into the conditional replacement vector pDELBOY-3X, a kind gift from D. J. Rossi, University of Helsinki (32). In order to flank the

exon 3 with *loxP* sites, a 2.7-kb EcoRI genomic fragment containing exon 3 was inserted into the ClaI/KpnI site of the targeting vector. The conditional replacement-type targeting vector containing the 14.5-kb mouse myotilin genomic DNA was linearized with NotI and electroporated into R1 ES cells (26). The 1.2-kb neomycin resistance gene in the targeting vector was used to select for homologous recombination. After G418 and ganciclovir selection, resistant clones were tested for correct targeting events by Southern blotting. Using BamHI-digested genomic DNA extracted from ES resistant clones, Southern blotting was performed with both 5′ and 3′ external probes of 2,300 bp and 2,000bp, respectively (Fig. 1B).

Correctly targeted ES cells were aggregated with ICR strain morulae, and two resulting chimeras were found to transmit the targeted allele through the germ line. The heterozygous floxed (hypomorph, or $myo^{flox/+}$) mice were bred with EIIa-Cre mice, ubiquitously expressing Cre recombinase under the cytomegalovirus promoter (18). The resulting myotilin $myo^{+/-}$ mice, heterozygous for the deleted allele, were subsequently intercrossed in order to obtain homozygous ($myo^{-/-}$) mice for the disrupted myotilin gene.

Genotyping of mice and RNA analysis. DNA was extracted from tail biopsy samples. Digested biopsy material was used for PCR genotyping, together with DyNAzyme II DNA polymerase (Finnzymes) and the following primers: Neo, 5′-GTCAGTTTCATAGCCTGAAGAACG-3′; NF3, 5′-CTTCTATTACCCTG CTCTGGGGTTG-3′; NR, 5′-CAAAGAGCCTTGTCGTCAAAGACCAGT-3′. PCR conditions were the following: denaturation at 95°C for 5 min, followed by 40 cycles of 45 s at 95°C, 1 min at 57°C, and 1 min 72°C, with a final extension of 10 min at 72°C. The NF3/NR pair of primers was used to amplify the wild-type and the floxed (hypomorphic) alleles of 350 and 450 bp, respectively. The pair Neo/NR was used to amplify a myotilin deleted allele of 500 bp.

Total RNA was isolated from hindlimb skeletal muscles using either the Chomczynski et al. method (3) or TRIzol (Invitrogen). A pool of 20 μg total RNA from $myo^{+/+}$, $myo^{+/-}$, and $myo^{-/-}$ mice ($n = 3$) was electrophoresed in a 1% denaturing agarose-formaldehyde gel, transferred to a Hybond-N^+ membrane (Amersham Biosciences), and subsequently heat fixed for 2 h at 80°C. The probes were random primed with [α-^{32}P]dCTP (Amersham Biosciences) using the Rediprime II labeling kit (Amersham Biosciences) and purified with Nick columns (Amersham Biosciences). The hybridizations were performed using ExpresHyb (Clontech) according to the manufacturer's instructions and high-stringency washed. Exon 3 was hybridized using a PCR-generated 192-bp probe corresponding to nucleotides (nt) 619 to 810, and exons 4, 5, and 6 were hybridized using a 255-bp probe corresponding to nt 823 to 1077. The 407-bp probe from the 3′-untranslated region of mouse telethonin corresponding to nt 539 to 945 was generated by PCR using mouse genomic DNA and the following pair of primers: 5′-GAGATGGACTGTGTGACTCAGA-3′ and 5′-CATGGCTGAGC ATTTATTGCAGTG-3′. A 991-bp mouse myopalladin probe was generated from mouse skeletal muscle RNA by reverse transcription-PCR (RT-PCR) using the primer 5′-GGCCGCAGTACAGTTCTGAAACCCAGTCCA-3′ and reverse 5′-TCTCTGTACCACTCGACTTTCGGAGATGGG-3′ and corresponds to a fragment, nt 605 to 1596, in the sequence with accession no. XM_978148. All probes generated by RT and RT-PCR were verified by sequencing. A β-actin probe of 2,000 bp from Clontech was used as a positive control and as a normalization signal when quantitative evaluation was done. The quantitative evaluation of the telethonin and myopalladin transcripts was done using ImageQuant TL version 2003.01 software on the data collected from a high-energy phosphor storage screen by using the Typhoon Scanner 9400 (Amersham Biosciences).

RNA isolated for Northern blotting was used for RT-PCR analysis. The cDNA strand was synthesized using random hexamers (Perkin-Elmer) and avian myeloblastosis virus reverse transcriptase (Finnzymes). Subsequently, myotilin-specific primers were used to amplify various myotilin fragments, as follows: exon 3 was amplified as a 192-bp fragment with forward primer 5′-GACTCCAACTA TCAACAATCC-3′ and reverse primer 5′-GGTCAGTCTTTGATTTCCA TATG −3′; a fragment consisting of 126 bp spanning exons 4 and 5 was amplified with forward primer 5′-ATGGCTCGCAGGTTGTTA-3′ and reverse primer 5′-TACTTGTGATGTGGG-3′; and the fragment of 343 bp flanking exon 3 was amplified with forward primer 5′-CAGCTTCCTCAGTTC-3′ and reverse primer 5′-ATCTTGGACATCACTGTT-3′. As a control, a 400-bp actin fragment was amplified from the same cDNA. The PCR with myotilin-specific primers was done with an initial denaturation step of 95°C for 5 min, followed by 40 cycles of the following steps: 94°C for 30 s, 55°C for 1 min, and 72°C for 1 min.

Western blot analysis. Skeletal muscle and heart tissue from $myo^{+/+}$, $myo^{+/-}$, and $myo^{-/-}$ mice were homogenized under liquid nitrogen, and the powder was solubilized in 8 M urea. Total protein concentration was measured by the Bradford 594-nm assay. Subsequently, equal quantities of proteins were separated onto 12% polyacrylamide minigels (Bio-Rad) and transferred on a nitrocellulose membrane (Schleicher & Schuell). Coomassie brilliant blue staining of the post-blotted gel was used to verify equal loading. After an overnight blocking at 4°C with 5% nonfat milk, 0.1% Tween 20 in phosphate-buffered saline (PBS), the membrane was probed with anti-myotilin 151 and 231 antibodies (1:2,000 dilution) (21) followed by horseradish peroxidase (HRP)-conjugated anti-rabbit antibodies (Dako) and detected with enhanced chemiluminescence (Amersham Biosciences). Other antibodies used for Western blot analysis were mouse polyclonal antitelethonin (1:500) (39), rat polyclonal anti-FATZ (1:800) (5), mouse polyclonal anti-ZASP (1:2,000) (6), monoclonal anti-sarcomeric α-actinin clone EA-53 (1:1,000; Sigma), mouse monoclonal anti-α-tubulin clone B-5-1-2 (1:5,000; Sigma), and monoclonal anti-actin AC40 antibody (1:12,000; Sigma). An antipalladin rabbit antibody, E1a, generated against an amino-terminal 16-residue peptide, was kindly provided by Markus Moser (Max Planck Institute of Biochemistry, Germany). The antiserum specifically recognizes an ~200-kDa band in the skeletal muscle, which corresponds to a predicted five-Ig domain palladin isoform transcribed from the most 5′ promoter of the palladin gene. The quantitation of protein bands was done using NIH Image 1.63 software (http://rsb.info.nih.gov/nih-image), and the total protein content was normalized by actin control immunoblot assays.

Morphological analysis of muscle specimens. Individual muscles of the hindlimb, forelimb, diaphragm, and heart were quickly removed after cervical dislocation. Each muscle was embedded separately in Tissue Tek (Sakura) and rapidly frozen in nitrogen-cooled isopentane (Sigma-Aldrich). Five-μm cryostat sections were placed on silanized SuperFrost glass slides (Menzel), acetone fixed, and stained with hematoxylin and eosin or by the modified Gomori trichrome method. For immunostaining, acetone-fixed cryosections were incubated for 1 hour at room temperature with polyclonal antimyotilin antibodies (151 or 231) diluted 1:300 in 3% bovine serum albumin in PBS, washed three times with PBS, and incubated for 30 min at room temperature with rhodamine anti-rabbit antibody (Jackson Immunoresearch Laboratories). Monoclonal anti-α-actinin EA-53 antibody was used at a 1:200 dilution, followed by Alexa 488 anti-mouse antibody (1:400; Molecular Probes). Slides were mounted with 1,4-diazabicyclo[2.2.2]octane (Sigma)-containing mounting medium. The sections were examined by immunofluorescence with a Zeiss Axiophot epifluorescence microscope (Carl Zeiss). Images were acquired with a Zeiss AxioCam cooled charge-coupled device camera and AxioVision software version 3.0.6 SP4 (Carl Zeiss).

Various organs (brain, abdominal muscles, spleen, lung, liver, kidney, skin, and small intestine) were collected from sacrificed adult mice. Sacrificed newborn (postnatal day 0) $myo^{-/-}$ ($n = 3$) and $myo^{+/+}$ ($n = 3$) mice and tissue specimens from adult mice were fixed in 10% formalin and processed using routine procedures for paraffin embedding, sectioning, and hematoxylin and eosin staining. A tail piece of newborn mice was sampled for DNA extraction and genotyping.

Transmission electron microscopy. For ultrastructural studies, tibialis anterior muscle and the cardiac apex were fixed in 4% glutaraldehyde in PBS and subsequently embedded in epoxy resin, ultrathin sectioned, and poststained using standard techniques (13).

Myofibril isolation. Bundles of myofibrils were isolated according to the method of Knight et al. (15) with small changes. Homogenized myofibrils were centrifuged onto silanized slides, fixed with methanol, and stained with anti-α-actinin and antimyotilin antibodies. The incubation times and dilutions used for staining were similar to those used for whole-muscle cryosections.

EBD injection. Vital dye Evans Blue (EBD; Sigma) was diluted 1% (wt/vol) in PBS, pH 7.5, and filtered through a 0.22-μm filter (Millipore). The mice were injected intraperitoneally with 1 mg EBD/0.1 ml PBS/10 g of body weight and euthanized by cervical dislocation 6 h later. The muscles were dissected, embedded individually in Tissue-Tek (Sakura), and rapidly frozen in nitrogen-cooled isopentane (Sigma-Aldrich). Cryostat sections of 5 μm were placed on silanized glass slides, acetone fixed, and observed with a Zeiss fluorescence microscope (Carl Zeiss) using 620-nm excitation.

Animal examination. The weight of $myo^{+/+}$, $myo^{+/-}$, and $myo^{-/-}$ mice was measured weekly starting from the weaning age (21 days) for 8 weeks and then measured monthly up to 38 months of age. Separately, the litters' weight from three breeding pairs was recorded weekly from day zero until the weaning age. Mice were monitored for changes in spontaneous behavior.

Muscle grip force measurements. Muscle strength was tested by 10 separate measurements using a grip meter attached to a force transducer, which measures peak force generated, and the data were recorded with PC-based software (TSE Systems). The instrument measures and records the peak pull force in pounds of the mouse's forelimbs and relies on the rodent's instinctive tendency to grab as it is pulled backward. The measurements were recorded for two groups according to the genotype of the mice, using both $myo^{+/+}$ and $myo^{+/-}$ mice as the control group. The strength was normalized according to the weight, and the results were plotted as mean values ± standard errors of the means (SEM).

Voluntary running. *myo*$^{-/-}$ (n = 5) and *myo*$^{+/+}$ (n = 4) control mice were placed individually in cages containing small metal running wheels connected to digital magnetic counters (BC 800 Sigma Sport). The mice were maintained under a standard light/dark cycle (12/12), fed ad libitum, and allowed free access to the wheel. Following an accommodation period of 10 days, the running activity was recorded for a total period of 5 weeks. The parameters collected were the daily running time and distance. Results were statistically processed using an unpaired t test and expressed as daily mean running time in hours ± standard deviation (SD), and daily mean running distance was expressed in kilometers ± SD. Upon termination of the exercise protocol, mice were sacrificed and skeletal muscles were collected and embedded for cryosectioning.

All animal experiments were performed according to the guidelines of protocols approved by the Animal Ethical Committee of the University of Helsinki.

RESULTS

Generation of gene-targeted *myotilin* null mice. In order to study the physiological role of myotilin during murine development and to explore myotilin's role in muscle structure and function, we generated a *myotilin* null mouse, *myo*$^{-/-}$. The targeted deletion of the murine *myotilin* gene consisted of in vivo Cre-*loxP*-mediated deletion of exon 3 ("floxing out") (18). We chose to delete exon 3 because it contains the second ATG in frame that might be translated into a truncated protein and because the engineered deletion introduced a stop codon at the joining region of exons 2 to 4. The strategy used was most likely to disrupt myotilin protein expression.

The heterozygous male floxed (*myo*$^{flox/+}$) mice were bred with EIIa-Cre transgenic general deletor females (17), and in vivo Cre-mediated excision of exon 3 was verified by PCR genotyping (Fig. 1C) and by Southern blotting (data not shown). Heterozygous (*myo*$^{+/-}$) mice bearing the exon 3-lacking allele (deleted allele) were intercrossed in order to obtain homozygous (*myo*$^{-/-}$) offspring. Different genotypes (*myo*$^{-/-}$, *myo*$^{+/-}$, and *myo*$^{+/+}$) were obtained at the expected Mendelian frequency. Widespread expression of myotilin during embryogenesis in several tissues is mainly documented in mice by in situ hybridization studies (22); however, at birth, the *myo*$^{-/-}$ mice were viable and indistinguishable by appearance, behavior (e.g., milk suckling, spontaneous movements), or average birth weight from their *myo*$^{+/-}$ or *myo*$^{+/+}$ littermates. For the analyses the mice were bred on a mixed 129SvJ/ICR background.

Expression of myotilin mRNA was investigated by RT-PCR and Northern blotting. Exon 3 primers did not amplify a PCR product from *myo*$^{-/-}$ skeletal muscle total RNA, whereas primers flanking the targeted exon 3 amplified a fragment that corresponded in size to the targeted deleted fragment (Fig. 2A). Instead, primers for downstream exons 4 and 5 amplified a product of expected size from the RNA of all genotypes.

In further Northern blotting experiments, skeletal muscle total RNA from *myo*$^{+/+}$, *myo*$^{+/-}$, and *myo*$^{-/-}$ mice (n = 3) was hybridized with an exon 3 probe and with a probe for exons 4, 5, and 6 (Fig. 2B). In the *myo*$^{-/-}$ skeletal muscle, no hybridization with the exon 3-specific probe was detected, verifying a successful in vivo recombination event and subsequent deletion of the targeted exon. Although RT-PCR suggested the presence of truncated myotilin RNA in *myo*$^{-/-}$ mice, we failed to detect exons located downstream of exon 3 by Northern blotting, indicating degradation of any myotilin transcript.

Myotilin protein analysis in *myo*$^{-/-}$ mice. Protein analysis of skeletal and cardiac muscle was done to confirm the absence of myotilin. Western blotting was performed with two different polyclonal antibodies recognizing the amino terminus or the first Ig-like domain of myotilin, respectively. Neither full-length nor truncated myotilin was detected in the *myo*$^{-/-}$ mice (Fig. 3A and data not shown). Other tissue types in the adult *myo*$^{+/+}$ mice did not contain detectable amounts of myotilin (data not shown).

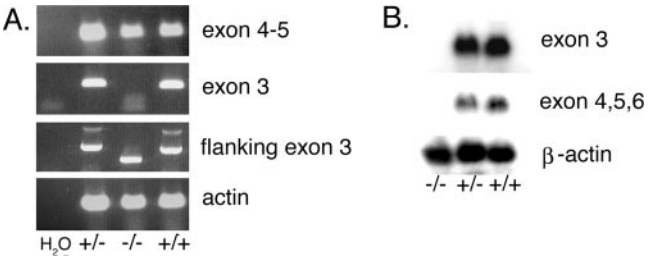

FIG. 2. RNA analysis of wild-type and *myo*$^{-/-}$ mice. A. Total skeletal muscle RNA was used as template for RT-PCR analysis. Exons 4 and 5 (126-bp fragment) were amplified in all samples. Exon 3 (192 bp) could be amplified from the *myo*$^{+/+}$ and *myo*$^{+/-}$ mouse RNA, but not from *myo*$^{-/-}$ mouse RNA. A 343-bp fragment flanking exon 3 was amplified form the *myo*$^{+/+}$ and heterozygous *myo*$^{+/-}$ mouse RNA, whereas a 175-bp fragment was amplified from *myo*$^{-/-}$ mice, further demonstrating the deletion of exon 3. The control lane on the left shows the RT-PCR in the absence of mouse RNA, and the bottom panel shows the actin RT-PCR as a control. B. Northern blot analysis of total RNA isolated from skeletal muscle of *myo*$^{-/-}$, *myo*$^{+/-}$, and *myo*$^{+/+}$ mice was performed with probes for exon 3 and for exons 4 to 6. The probes did not detect any myotilin transcript in *myo*$^{-/-}$ mice. A β-actin probe is shown as a total RNA loading control.

Expression of other Z-disk proteins in *myo*$^{-/-}$ striated muscle. Quantitative Western blot analysis was used to assess the expression of several Z-disk-associated proteins. The investigation showed minor, if any, changes in α-actinin, two major ZASP isoforms (of 36 kDa and 78 kDa), or FATZ-1 expression in the *myo*$^{-/-}$ mouse skeletal (Fig. 3A) or cardiac (not shown) muscle. Instead, a notable increase was observed in expression of telethonin in skeletal muscle and a minor increase was seen in cardiac muscle (Fig. 3A). Quantitative analysis of skeletal and cardiac muscle blots demonstrated a nearly 2-fold and 1.6-fold increase, respectively, of telethonin protein in the *myo*$^{-/-}$ mice (Fig. 3B). Similarly, quantitative Northern blot analysis of telethonin with a 3′-untranslated region probe indicated upregulated telethonin RNA in *myo*$^{-/-}$ skeletal muscle (data not shown). We also investigated the presence of the ~200-kDa major palladin isoform reported to be present in mouse embryonic heart and skeletal muscle (29). An antibody that specifically recognizes the amino terminus of palladin did not indicate differences in the signal intensity between *myo*$^{-/-}$ and *myo*$^{+/+}$ mice (Fig. 3C). In the absence of a suitable antibody, expression of the third subfamily member, myopalladin, was analyzed by Northern blotting. The results showed that an equal amount of myopalladin transcript was present in the striated muscles of *myo*$^{-/-}$ mice and the *myo*$^{+/+}$ controls (Fig. 3D).

Morphology and sarcolemmal integrity of skeletal muscle and heart in *myo*$^{-/-}$ mice. The morphology of skeletal and cardiac muscle was investigated by light microscopy and transmission electron microscopy. Histological evaluation was done by comparing hematoxylin and eosin-stained sections of skel-

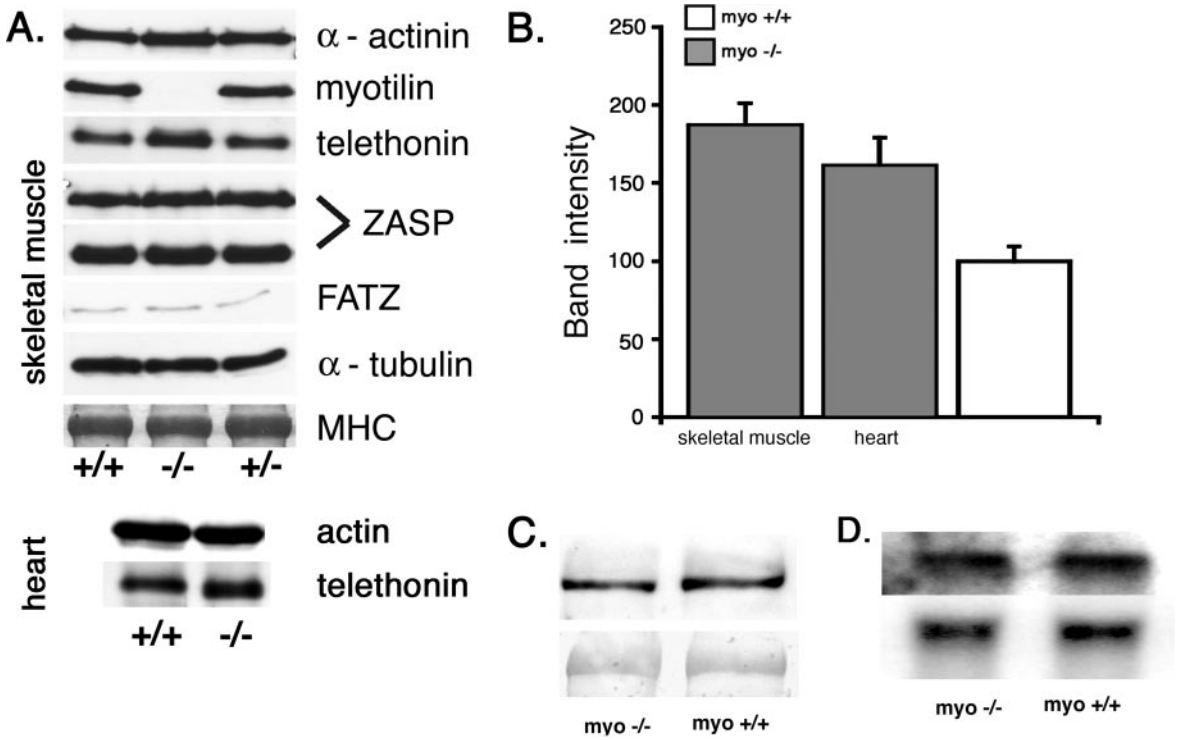

FIG. 3. Immunoblot and Northern blot analysis of muscle proteins. A. The presence of Z-disk proteins was investigated by immunoblotting using crude skeletal and cardiac muscle homogenates of $myo^{+/+}$, $myo^{-/-}$, and $myo^{+/-}$ mice. The immunoblot with antimyotilin antibody 151 shows lack of reactivity in the $myo^{-/-}$ muscle, indicating the absence of the protein. α-Actinin, ZASP (32-kDa and 78-kDa isoforms), FATZ-1, and α-tubulin are normally expressed. Instead, a markedly increased telethonin reactivity is observed in the skeletal muscle and a minor increase is detected in the cardiac muscle. Myosin heavy chain (MHC) detection using Coomassie staining of the postblotted gel served as a loading control. B. Quantification of telethonin content in skeletal and cardiac muscle of $myo^{-/-}$ mice. Western blot intensity of the telethonin signal ($n = 3$) was normalized to the actin content detected with the monoclonal AC40 antibody. The data obtained from nine measurements are reported as means + SEM of the telethonin content in the $myo^{+/+}$ skeletal or cardiac muscles, which was assigned 100 (SEM = 14.26). C. Western blot analysis of an ~200-kDa muscle palladin isoform in skeletal muscles. The upper panel shows equal amounts of palladin detected with E1a antibody. The lower panel shows Ponceau S-stained nitrocellulose membrane to illustrate an equal amount of protein loading. D. Northern blot analysis of myopalladin transcript in the skeletal muscle. The upper panel is the myopalladin probe, and the lower panel is a β-actin probe used as a loading control.

etal muscles of various genotypes from postnatal day zero to 50-week-old mice. Neonatal mice were investigated for possible delayed muscle development of the limb muscles, diaphragm, or heart. The morphology of muscle groups or individual muscle fibers did not differ in the neonatal $myo^{-/-}$ mice compared with the $myo^{+/+}$ mice. In the adult stage, we could not detect any dystrophic features or other morphological abnormalities (Fig. 4A) in the skeletal and cardiac muscle. Gomori trichrome staining was used to detect abnormal deposits, such as nemaline rods or tubular aggregates. Occasional small accumulations were detected in the skeletal muscle of both male $myo^{-/-}$ and $myo^{+/+}$ mice after 6 months (not shown). Such structures are known to appear in an age-dependent manner in the skeletal muscles of inbred male mice (1). The gender selectivity, the presence in the control samples, and studies showing that they originate from sarcoplasmic reticulum or/and mitochondria (1, 27) supported the observation that they were not a specific morphological change in skeletal muscles of $myo^{-/-}$ mice.

The ultrastructure of skeletal and cardiac muscle was further assessed by transmission electron microscopy. The sarcomere and the Z-disks in $myo^{-/-}$ mice were structurally preserved, and there was no indication of Z-disk streaming, dissolution, or accumulation of filamentous material in either muscle type (Fig. 4B).

Immunofluorescence analysis of isolated myofibrils was performed to further verify the absence of myotilin and to investigate maintenance of the sarcomeric architecture in the $myo^{-/-}$ mice. The Z-disk protein α-actinin was detected in myofibrils prepared from $myo^{-/-}$ and $myo^{+/+}$ mouse skeletal muscles. The pattern showed characteristic striations that correspond to the periodical Z-disk structure both in $myo^{+/+}$ myofibrils and in $myo^{-/-}$ myofibrils, which lack immunoreactivity for myotilin (Fig. 4C). The normal Z-disk striated pattern was verified by immunofluorescence staining using a titin antibody recognizing the Z-disk epitope of titin (data not shown).

Dystrophic patients with myotilin mutations show increased serum creatine kinase levels, which may indicate an increased sarcolemmal permeability. To explore the integrity of the sarcolemma, the intravital dye EBD (11) was used as an alternative method for measuring circulating creatine kinase levels. The $myo^{-/-}$ mice did not display an increased EBD uptake, suggesting that the sarcolemmal integrity was not affected (data not shown).

Postnatal growth curve of $myo^{-/-}$ mice. The growth curve serves as a general measure of health, especially in the periods

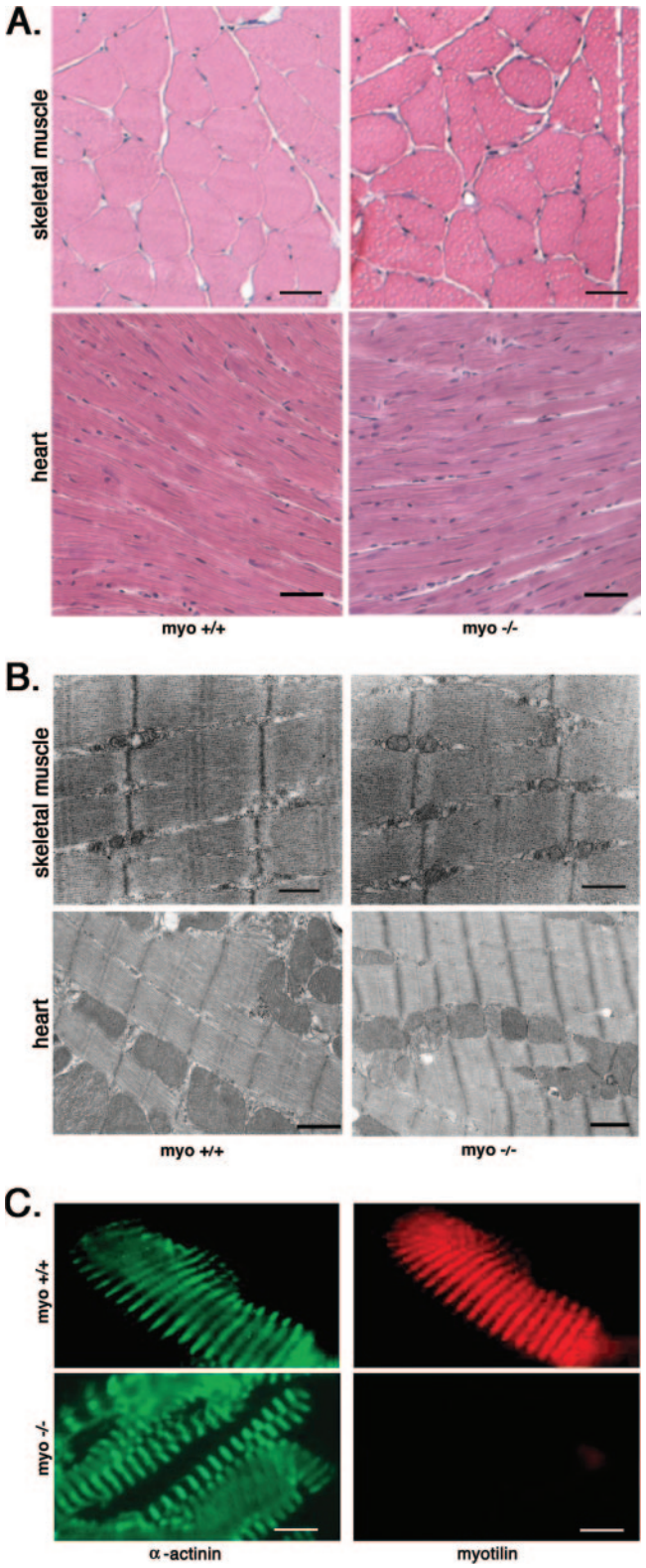

FIG. 4. Morphological analysis of $myo^{+/+}$ and $myo^{-/-}$ skeletal and cardiac muscle. A. The upper panel shows transversal cryosections of gastrocnemius from 12-month-old $myo^{+/+}$ and $myo^{-/-}$ mice, stained with hematoxylin and eosin. The lower panel shows morphology of the heart. No morphological differences were seen in either muscle type. Bar, 20 μm. B. Ultrastructural analysis of the $myo^{-/-}$ mouse skeletal and cardiac muscle shows an unaffected morphology of the sarcomere. The Z-disk, observed as a dark line, is not changed in the $myo^{-/-}$ mice compared with $myo^{+/+}$ mice. Bar, 500 nm. C. Immunofluorescence staining of isolated myofibrils shows Z-disk myotilin staining in $myo^{+/+}$ mice but not in the $myo^{-/-}$ muscles. Staining of α-actinin demonstrates normal Z-disk distribution in $myo^{-/-}$ skeletal muscle. Bar, 20 μm.

of rapid growth (i.e., after weaning) (4). The postnatal period from day zero to 3 weeks was characterized by a similar growth rate of both genotypes (Fig. 5A). Towards weaning and during the postweaning period the growth curves remained similar, demonstrating a difference between genders but not between genotypes (Fig. 5B). During the analyses, the spontaneous behavior of the mice was also observed. The behavior of the $myo^{-/-}$ mice was not different from that of the controls throughout their life span, and no deaths based on cardiac pathology were recorded.

Morphology of other tissue types in $myo^{-/-}$ mice. As myotilin is expressed in several organs during development, we compared the morphology of several nonmuscle organs in $myo^{-/-}$ mice and their littermates at birth and during adult age. Analysis of hematoxylin and eosin-stained tissue sections did not reveal any morphological differences between the genotypes in brain, spleen, kidney, lung, liver, skin, or small intestine (not shown).

Loss of myotilin does not affect muscle strength or interfere with daily performance. In order to investigate the functional consequence of myotilin absence in the tissues that express myotilin abundantly, measurements of strength and fatigue were performed. Figure 5C shows forelimb peak force measurements of >10-month-old mice. Four trials were performed at 1-week intervals. Each trial consisted of 10 measurements, and the values were plotted as a function of weight. An insignificantly reduced strength was measured in the $myo^{-/-}$ mice, in comparison with $myo^{+/+}$ mice (Fig. 5C). These results indicate that, in addition to the normal morphology of the sarcomere, normal maximal contractile function is retained in spite of loss of myotilin. In addition, we compared the endurance capacity of $myo^{-/-}$ and $myo^{+/+}$ mice and tested whether exercise affected muscle morphology. The performance was assessed using the voluntary running exercise (2). The results showed a small but insignificant reduction in the voluntary running activity of $myo^{-/-}$ mice. Mice lacking myotilin ran an average of 2.12 ± 0.44 h/day (compared to 2.40 ± 1.56 h/day) at an average distance of 3.04 ± 2.20 kilometers/day (compared to 3.89 ± 3.05 kilometers/day) (Fig. 5D and E). After the exercise period, the skeletal muscle morphology of both $myo^{-/-}$ and $myo^{+/+}$ mice showed increased fiber size (2). However, no signs of degeneration/regeneration or other muscle pathology were detected (data not shown).

DISCUSSION

Myotilin is a recently described actin-associated sarcomeric protein that is highly conserved between human and mouse (21). Although its molecular associations and in vitro functions have been described and mutations in the *myotilin* gene have been shown to cause muscular disorders, myotilin's role in vivo has not yet been explored. In this paper, we report that lack of

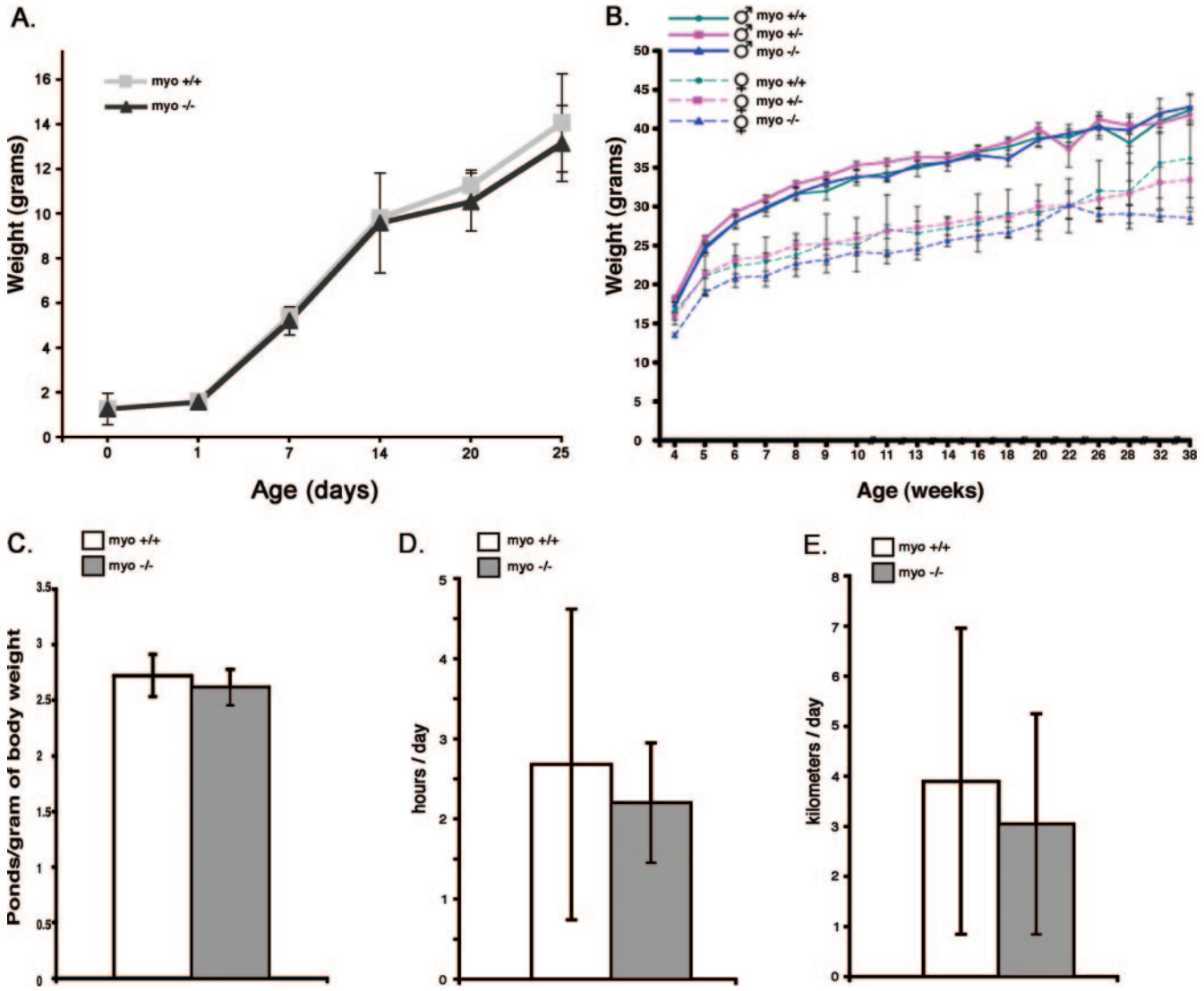

FIG. 5. Growth curves, grip strength measurements, and endurance of $myo^{+/+}$ and $myo^{-/-}$ mice. A. Weights of $myo^{-/-}$ and $myo^{+/+}$ mice from birth to postnatal day 25. The genotypes have identical birth weights and develop similarly. Each data point value depicts the mean value ± SEM. B. Postweaning weight curves are depicted separately for each genotype and sex until 38 weeks of age. The intensive growth phase and the adult period show gender differences but are not affected by genotype. Each data point depicts the mean value ± SEM. C. Forelimb grip strength of >10-month-old male $myo^{-/-}$ mice ($n = 7$) was compared with that of a group of gender- and age-matched $myo^{+/+}$ mice. The grip strength from four trials, each consisting of 10 pulls, was normalized to the average body weight. The mean values are presented as column plots ± SEM. The $myo^{-/-}$ mice showed an insignificant decrease of strength compared with the age- and sex-matched control group. D and E. Running performance of $myo^{-/-}$ and $myo^{+/+}$ mice. Daily voluntary running of $myo^{-/-}$ mice ($n = 5$) compared with the $myo^{+/+}$ ($n = 4$) mice is expressed as the average daily running time (D) and distance (E). $myo^{-/-}$ mice showed a small but statistically insignificant reduction in running time and distance. The data are shown as the average ± SD.

myotilin does not cause phenotypic alterations in $myo^{-/-}$ mice. The knockout mice demonstrated a normal ultrastructure of skeletal and cardiac muscle, unaffected distribution of Z-disk proteins, normal muscle function, and a normal life span.

Our results indicate that myotilin is not required for murine development. This is in contrast to palladin, a structurally related molecule, whose ablation results in embryonic lethality due to defects in ventral and dorsal tube closure (19). The phenotype of the third family member, myopalladin, has not been reported. The lack of phenotype in $myo^{-/-}$ mice suggests that palladin and/or myopalladin serve overlapping functions with myotilin and thereby can functionally compensate its loss. In contrast, myotilin and myopalladin cannot compensate for loss of palladin in many cell types, since palladin has a much broader expression pattern than the two other family members.

The maintenance of a morphologically normal Z-disk and overall cellular architecture, the absence of inflammatory or degeneration/regeneration features, and preserved muscle performance of $myo^{-/-}$ animals confirmed that lack of myotilin does not lead to a dystrophic phenotype. The normal morphology and function of the skeletal muscle of $myo^{-/-}$ mice up to old age indicated that myotilin is not required for normal

striated muscle structure and gross function, including muscle force and endurance. Generation of double or triple knockout mice by deletion of myopalladin and/or muscle-specific palladin may be necessary in order to analyze the redundant roles of the proteins forming this small subfamily.

Although *myo*$^{-/-}$ muscles were morphologically indistinguishable from wild type, differences in their molecular composition were detected. Specifically, we observed upregulation of another Z-disk protein, telethonin/T-cap (20, 39), at both the protein and mRNA level. The upregulation was more pronounced in skeletal than in cardiac muscle. The Z-disk not only provides a scaffold for the contractile units, but it also serves an important role as a mechanosensor and mediator of signaling (31). Telethonin binds the giant protein titin at the Z-disk periphery (24). In addition, it is suggested that telethonin cross-links titin's amino termini in a way which results in unique spatial organization of filaments within the sarcomere and increased Z-disk resistance to contractive stress (44). In heart, telethonin binds in a phosphorylation-dependent manner the potassium channel β-subunit minK, localized to the T-tubular system. The complex formed by telethonin/T-cap together with the Z-disk amino terminus of titin and minK is proposed as a part of a "mechano-electrical feedback" linking mechanical stretch with membrane potentials (9). Mutations in the telethonin gene underlie an autosomal recessive form of limb girdle muscular dystrophy, LGMD2G (23), and dilated cardiomyopathy (16), but these patients do not display Z-disk alterations (38). Telethonin is thought to be linked to the dynamic control of myofibrillogenesis and muscle turnover (35). It is also considered an important player in stretch sensing, providing the necessary feedback for Z-disk key proteins (16). Thus, its changed expression profile in the *myo*$^{-/-}$ mouse skeletal muscle could reflect a structural weakening of the Z-disk supporting, at least in part, the documented role of myotilin as a cross-linker. Alternatively, telethonin upregulation could be considered a marker of altered mechanosensing, which could indicate a new role for myotilin as a component of the muscle stretch-sensing molecular pathway. Nevertheless, more studies are needed in order to demonstrate myotilin's role as an active component of the Z-disk structure and function.

Recently, mouse knockout studies of Z-disk proteins structurally or functionally linked with myotilin have been reported. The gene ablation strategy for FATZ 2/calsarcin-1, a binding partner of myotilin, served as a good tool for investigating the protein's cellular functions. The calsarcin-1 knockout mouse displayed an apparently normal phenotype, but exaggerated cardiac hypertrophy was seen in response to calcineurin activation (8). The actinin-associated LIM domain protein (ALP) is a PDZ and LIM domain-containing protein that localizes to the Z-disks of skeletal and, to a lesser extent, of cardiac muscle. The ALP null mouse did not display a skeletal muscle phenotype (14); however, subtle cardiac morphological changes and dysfunction were reported in another study (30). The mouse homologue of human ZASP, Cypher/Oracle, is a member of the PDZ-LIM domain-containing protein family. Along with mutations in myotilin and some other Z-disk proteins, ZASP mutations can cause myofibrillar myopathy (37). Interestingly, knockout studies indicate that Cypher/ZASP is not required for sarcomerogenesis but for the maintenance of Z-disk integrity during muscle contraction, as ablation of Cypher1 and Cypher2 results in a severe form of congenital myopathy and ventricular dilatation (43). Only minor changes were seen in the endurance of *myo*$^{-/-}$ mice during physical stress. Perhaps an even more challenging environment may be needed in order to reveal subtle changes in *myo*$^{-/-}$ mice.

Myotilin mutations cause several forms of myotilinopathy, defined by clinical and morphological features as LGMD1A (13, 12), myofibrillar myopathy (36, 28), and spheroid body myopathy (7). To date, point mutations in the *myotilin* gene are clustered within exon 2 and result in single amino acid changes in a serine-rich amino-terminal region of myotilin. Interestingly, several of the mutated residues are putative phosphorylation sites. The significance of the point mutation still awaits clarification, as transfection studies in nonmuscle cells show that myotilin proteins carrying several disease-associated mutations could still be found associated with actin filaments (41). Together, the human disease spectrum and the results of this paper support the hypothesis that mutated myotilin serves a dominant negative function in striated muscle. This could explain why mutations in the *myotilin* gene leading to protein absence have not been found among the human muscular dystrophy disease spectrum.

ACKNOWLEDGMENTS

We thank H. Ahola for skilled technical assistance.

This work was supported by CIMO, the Academy of Finland, the Finnish Cultural Foundation, the Finnish Heart Association, TEKES, and grant GGP04088 from the Telethon Foundation, Italy, to G.F.

REFERENCES

1. **Agbulut, O., J. Destombes, D. Thiesson, and G. Butler-Browne.** 2000. Age-related appearance of tubular aggregates in the skeletal muscle of almost all male inbred mice. Histochem. Cell Biol. **114:**477–481.
2. **Allen, D. L., B. C. Harrison, A. Maass, M. L. Bell, W. C. Byrnes, and L. A. Leinwand.** 2001. Cardiac and skeletal muscle adaptations to voluntary wheel running in the mouse. J. Appl. Physiol. **90:**1900–1908.
3. **Chomczynski, P., and N. Sacchi.** 1987. Single-step method of RNA isolation by acid guanidinium thiocyanate-phenol-chloroform extraction. Anal. Biochem. **162:**156–159.
4. **Connolly, A. M., R. M. Keeling, S. Mehta, A. Pestronk, and J. R. Sanes.** 2001. Three mouse models of muscular dystrophy: the natural history of strength and fatigue in dystrophin-, dystrophin/utrophin-, and laminin α2-deficient mice. Neuromuscul. Disord. **11:**703–712.
5. **Faulkner, G., A. Pallavicini, A. Comelli, M. Salamon, G. Bortoletto, C. Ievolella, S. Trevisan, S. Kojic, F. Dalla Vecchia, P. Laveder, G. Valle, and G. Lanfranchi.** 2000. FATZ, a filamin-, actinin-, and telethonin-binding protein of the Z-disc of skeletal muscle. J. Biol. Chem. **275:**41234–41242.
6. **Faulkner, G., A. Pallavicini, E. Formentin, A. Comelli, C. Ievolella, S. Trevisan, G. Bortoletto, P. Scannapieco, M. Salamon, V. Mouly, G. Valle, and G. Lanfranchi.** 1999. ZASP: a new Z-band alternatively spliced PDZ-motif protein. J. Cell Biol. **146:**465–475.
7. **Foroud, T., N. Pankratz, A. P. Batchman, M. W. Pauciulo, R. Vidal, L. Miravalle, H. H. Goebel, L. J. Cushman, B. Azzarelli, H. Horak, M. Farlow, and W. C. Nichols.** 2005. A mutation in myotilin causes spheroid body myopathy. Neurology **65:**1936–1940.
8. **Frey, N., T. Barrientos, J. M. Shelton, D. Frank, H. Rütten, D. Gehring, C. Kuhn, M. Lutz, B. Rothermel, R. Bassel-Duby, J. A. Richardson, H. A. Katus, J. A. Hill, and E. N. Olson.** 2004. Mice lacking calsarcin-1 are sensitized to calcineurin signaling and show accelerated cardiomyopathy in response to pathological biomechanical stress. Nat. Med. **10:**1336–1343.
9. **Furukawa, T., Y. Ono, H. Tsuchiya, Y. Katayama, M. L. Bang, D. Labeit, S. Labeit, N. Inagaki, and C. C. Gregorio.** 2001. Specific interaction of the potassium channel beta-subunit minK with the sarcomeric protein T-cap suggests a T-tubule-myofibril linking system. J. Mol. Biol. **313:**775–784.
10. **Gontier, Y., A. Taivainen, L. Fontao, A. Sonnenberg, A. van der Flier, O. Carpén, G. Faulkner, and L. Borradori.** 2005. The Z-disc proteins myotilin and FATZ-1 interact with each other and are connected to the sarcolemma via muscle-specific filamins. J. Cell Sci. **118:**3739–3749.
11. **Hamer, P. W., J. M. McGeachie, M. J. Davies, and M. D. Grounds.** 2002. Evans blue dye as an in vivo marker of myofibre damage: optimising

parameters for detecting initial myofibre membrane permeability. J. Anat. **200:**69–79.
12. **Hauser, M. A., C. B. Conde, V. Kowaljow, G. Zeppa, A. L. Taratuto, U. M. Torian, J. Vance, M. A. Pericak-Vance, M. C. Speer, and A. L. Rosa.** 2002. *myotilin* mutation found in second pedigree with LGMD1A. Am. J. Hum. Genet. **71:**1428–1432.
13. **Hauser, M. A., S. K. Horrigan, P. Salmikangas, U. M. Torian, K. D. Viles, R. Dancel, R. W. Tim, A. Taivainen, L. Bartoloni, J. M. Gilchrist, J. M. Stajich, P. C. Gaskell, J. R. Gilbert, J. M. Vance, M. A. Pericak-Vance, O. Carpén, C. A. Westbrook, and M. C. Speer.** 2000. Myotilin is mutated in limb girdle muscular dystrophy 1A. Hum. Mol. Genet. **9:**2141–2147.
14. **Jo, K., B. Rutten, R. C. Bunn, and D. S. Bredt.** 2001. Actinin-associated LIM protein-deficient mice maintain normal development and structure of skeletal muscle. Mol. Cell. Biol. **21:**1682–1687.
15. **Knight, P. J., and J. A. Trinick.** 1982. Preparation of myofibrils. Methods Enzymol. **85**(Pt. B)**:**9–12.
16. **Knöll, R., M. Hoshijima, H. M. Hoffman, V. Person, I. Lorenzen-Schmidt, M. L. Bang, T. Hayashi, N. Shiga, H. Yasukawa, W. Schaper, W. McKenna, M. Yokoyama, N. J. Schork, J. H. Omens, A. D. McCulloch, A. Kimura, C. C. Gregorio, W. Poller, J. Schaper, H. P. Schultheiss, and K. R. Chien.** 2002. The cardiac mechanical stretch sensor machinery involves a Z disc complex that is defective in a subset of human dilated cardiomyopathy. Cell **111:**943–955.
17. **Lakso, M., J. G. Pichel, J. R. Gorman, B. Sauer, Y. Okamoto, E. Lee, F. W. Alt, and H. Westphal.** 1996. Efficient in vivo manipulation of mouse genomic sequences at the zygote stage. Proc. Natl. Acad. Sci. USA **93:**5860–5865.
18. **Lallemand, Y., V. Luria, R. Haffner-Krausz, and P. Lonai.** 1998. Maternally expressed PGK-Cre transgene as a tool for early and uniform activation of the Cre site-specific recombinase. Transgenic Res. **7:**105–112.
19. **Luo, H., X. Liu, F. Wang, Q. Huang, S. Shen, L. Wang, G. Xu, X. Sun, H. Kong, M. Gu, S. Chen, Z. Chen, and Z. Wang.** 2005. Disruption of palladin results in neural tube closure defects in mice. Mol. Cell Neurosci. **29:**507–515.
20. **Mason, P., S. Bayol, and P. T. Loughna.** 1999. The novel sarcomeric protein telethonin exhibits developmental and functional regulation. Biochem. Biophys. Res. Commun. **257:**699–703.
21. **Mologni, L., M. Moza, M. M. Lalowski, and O. Carpén.** 2005. Characterization of mouse myotilin and its promoter. Biochem. Biophys. Res. Commun. **329:**1001–1009.
22. **Mologni, L., P. Salmikangas, F. Fougerousse, J. S. Beckmann, and O. Carpén.** 2001. Developmental expression of myotilin, a gene mutated in limb-girdle muscular dystrophy type 1A. Mech. Dev. **103:**121–125.
23. **Moreira, E. S., T. J. Wiltshire, G. Faulkner, A. Nilforoushan, M. Vainzof, O. T. Suzuki, G. Valle, R. Reeves, M. Zatz, M. R. Passos-Bueno, and D. E. Jenne.** 2000. Limb-girdle muscular dystrophy type 2G is caused by mutations in the gene encoding the sarcomeric protein telethonin. Nat. Genet. **24:**163–166.
24. **Mues, A., P. F. van der Ven, P. Young, D. O. Fürst, and M. Gautel.** 1998. Two immunoglobulin-like domains of the Z-disc portion of titin interact in a conformation-dependent way with telethonin. FEBS Lett. **428:**111–114.
25. **Mykkänen, O. M., M. Grönholm, M. Rönty, M. Lalowski, P. Salmikangas, H. Suila, and O. Carpén.** 2001. Characterization of human palladin, a microfilament-associated protein. Mol. Biol. Cell **12:**3060–3073.
26. **Nagy, A., J. Rossant, R. Nagy, W. Abramow-Newerly, and J. C. Roder.** 1993. Derivation of completely cell culture-derived mice from early-passage embryonic stem cells. Proc. Natl. Acad. Sci. USA **90:**8424–8428.
27. **Novotova, M., I. Zahradnik, G. Brochier, M. Pavlovicova, X. Bigard, and R. Ventura-Clapier.** 2002. Joint participation of mitochondria and sarcoplasmic reticulum in the formation of tubular aggregates in gastrocnemius muscle of $CK^{-/-}$ mice. Eur. J. Cell Biol. **81:**101–106.
28. **Olivé, M., L. G. Goldfarb, A. Shatunov, D. Fischer, and I. Ferrer.** 2005. Myotilinopathy: refining the clinical and myopathological phenotype. Brain **128:**2315–2326.
29. **Otey, C. A., A. Rachlin, M. Moza, D. Arneman, and O. Carpén.** 2005. The palladin/myotilin/myopalladin family of actin-associated scaffolds. Int. Rev. Cytol. **246:**31–58.
30. **Pashmforoush, M., P. Pomiès, K. L. Peterson, S. Kubalak, J. Ross Jr., A. Hefti, U. Aebi, M. C. Beckerle, and K. R. Chien.** 2001. Adult mice deficient in actinin-associated LIM-domain protein reveal a developmental pathway for right ventricular cardiomyopathy. Nat. Med. **7:**591–597.
31. **Pyle, W. G., and R. J. Solaro.** 2004. At the crossroads of myocardial signaling: the role of Z-discs in intracellular signaling and cardiac function. Circ. Res. **94:**296–305.
32. **Rossi, D. J., A. Londesborough, N. Korsisaari, A. Pihlak, E. Lehtonen, M. Henkemeyer, and T. P. Mäkelä.** 2001. Inability to enter S phase and defective RNA polymerase II CTD phosphorylation in mice lacking Mat1. EMBO J. **20:**2844–2856.
33. **Salmikangas, P., O. M. Mykkänen, M. Grönholm, L. Heiska, J. Kere, and O. Carpén.** 1999. Myotilin, a novel sarcomeric protein with two Ig-like domains, is encoded by a candidate gene for limb-girdle muscular dystrophy. Hum. Mol. Genet. **8:**1329–1336.
34. **Salmikangas, P., P. F. van der Ven, M. Lalowski, A. Taivainen, F. Zhao, H. Suila, R. Schröder, P. Lappalainen, D. O. Fürst, and O. Carpén.** 2003. Myotilin, the limb-girdle muscular dystrophy 1A (LGMD1A) protein, cross-links actin filaments and controls sarcomere assembly. Hum. Mol. Genet. **12:**189–203.
35. **Schröder, R., J. Reimann, A. Iakovenko, A. Mues, C. G. Bonnemann, J. Matten, and M. Gautel.** 2001. Early and selective disappearance of telethonin protein from the sarcomere in neurogenic atrophy. J. Muscle Res. Cell. Motil. **22:**259–264.
36. **Selcen, D., and A. G. Engel.** 2004. Mutations in myotilin cause myofibrillar myopathy. Neurology **62:**1363–1371.
37. **Selcen, D., and A. G. Engel.** 2005. Mutations in ZASP define a novel form of muscular dystrophy in humans. Ann. Neurol. **57:**269–276.
38. **Vainzof, M., E. S. Moreira, O. T. Suzuki, G. Faulkner, G. Valle, A. H. Beggs, O. Carpén, A. F. Ribeiro, E. Zanoteli, J. Gurgel-Gianneti, A. M. Tsanaclis, H. C. Silva, M. R. Passos-Bueno, and M. Zatz.** 2002. Telethonin protein expression in neuromuscular disorders. Biochim. Biophys. Acta **1588:**33–40.
39. **Valle, G., G. Faulkner, A. De Antoni, B. Pacchioni, A. Pallavicini, D. Pandolfo, N. Tiso, S. Toppo, S. Trevisan, and G. Lanfranchi.** 1997. Telethonin, a novel sarcomeric protein of heart and skeletal muscle. FEBS Lett. **415:**163–168.
40. **van der Ven, P. F., S. Wiesner, P. Salmikangas, D. Auerbach, M. Himmel, S. Kempa, K. Hayess, D. Pacholsky, A. Taivainen, R. Schröder, O. Carpén, and D. O. Fürst.** 2000. Indications for a novel muscular dystrophy pathway. gamma-filamin, the muscle-specific filamin isoform, interacts with myotilin. J. Cell Biol. **151:**235–248.
41. **von Nandelstadh, P., M. Grönholm, M. Moza, A. Lamberg, H. Savilahti, and O. Carpén.** 2005. Actin-organising properties of the muscular dystrophy protein myotilin. Exp. Cell Res. **310:**131–139.
42. **Witt, S. H., H. Granzier, C. C. Witt, and S. Labeit.** 2005. MURF-1 and MURF-2 target a specific subset of myofibrillar proteins redundantly: towards understanding MURF-dependent muscle ubiquitination. J. Mol. Biol. **350:**713–722.
43. **Zhou, Q., P. H. Chu, C. Huang, C. F. Cheng, M. E. Martone, G. Knoll, G. D. Shelton, S. Evans, and J. Chen.** 2001. Ablation of Cypher, a PDZ-LIM domain Z-line protein, causes a severe form of congenital myopathy. J. Cell Biol. **155:**605–612.
44. **Zou, P., N. Pinotsis, S. Lange, Y. H. Song, A. Popov, I. Mavridis, O. M. Mayans, M. Gautel, and M. Wilmanns.** 2006. Palindromic assembly of the giant muscle protein titin in the sarcomeric Z-disk. Nature **439:**229–233.